Quantum reservoir complexity by the Krylov evolution approach

Laia Domingo [1,2,3,*] F. Borondo [1,†] Gastón Scialchi [4] Augusto J. Roncaglia[4]
Gabriel G. Carlo,[5,‡] and Diego A. Wisniacki[4,§]

[1]*Departamento de Química, Universidad Autónoma de Madrid, CANTOBLANCO - 28049 Madrid, Spain*
[2]*Grupo de Sistemas Complejos, Universidad Politécnica de Madrid, 28035 Madrid, Spain*
[3]*Instituto de Ciencias Matemáticas (ICMAT), Campus de Cantoblanco, Universidad Autónoma de Madrid,
Nicolás Cabrera 13-15, 28049 Madrid, Spain*
[4]*Universidad de Buenos Aires, Facultad de Ciencias Exactas y Naturales, Departamento de Física, 1428 Buenos Aires, Argentina
and CONICET - Universidad de Buenos Aires, Instituto de Física de Buenos Aires (IFIBA), 1428 Buenos Aires, Argentina*
[5]*Departamento de Física, Comisión Nacional de Energía Atómica, Avenida del Libertador 8250, (C1429BNP) Buenos Aires, Argentina*

Quantum reservoir computing algorithms recently emerged as a standout approach in the development of successful methods for the noisy intermediate-scale quantum (NISQ) era because of its superb performance and compatibility with current quantum devices. By harnessing the properties and dynamics of a quantum system, quantum reservoir computing effectively uncovers hidden patterns in data. However, the design of the quantum reservoir is crucial to this end in order to ensure an optimal performance of the algorithm. In this work, we introduce a precise quantitative method with strong physical foundations based on the Krylov evolution to assess the wanted good performance in machine-learning tasks. Our results show that the Krylov approach to complexity strongly correlates with quantum reservoir performance, making it a powerful tool in the quest for optimally designed quantum reservoirs, which will pave the road to the implementation of successful quantum machine-learning methods.

I. INTRODUCTION

Quantum computing is currently a rapidly evolving field, exerting a substantial impact on various domains, including cryptography, optimization, and machine learning. Despite remarkable recent progress, the development of fault-tolerant quantum computers, capable of solving most challenging tasks such as integer factorization [1] or unstructured search [2], remains a long-term goal that necessitates extensive error correction for a significant number of qubits. As an interesting alternative, noisy intermediate-scale quantum (NISQ) [3] algorithms, which leverage the current generation of quantum computers with tens or hundreds of qubits, have recently accomplished important milestones [4].

A promising application of NISQ devices is quantum machine learning. Machine learning focuses on developing algorithms to learn from and make predictions based on data, without being explicitly programed. In particular, quantum reservoir computing (QRC) [5,6] has emerged as a powerful algorithm, demonstrating an excellent performance on a wide range of applications [7–11]. Notably, QRC represents a significant leap in the realm of machine learning, built upon the foundations of classical reservoir computing [12]. While classical reservoir computing relies on the dynamic properties

of neural networks for computational tasks, QRC exploits the dynamics and properties of characteristic quantum systems as computational resources to perform machine-learning tasks [13,14]. These dynamics have been recently shown to play a key role in the efficiency of QRC [7], and the main goal of this work is to provide an adequate venue for its optimal design, which allows the processing of larger input datasets taking advantage of the exponential size of the associated Hilbert space. Within this framework, QRC has been able to solve multiple problems within classification, regression and temporal tasks. These include tasks like image classification [15], electronic energy computation for quantum chemistry [10,16], and time series forecasting [6,9,17–21].

In gate-based quantum computing, QRC relies on a random quantum circuit, also known as the *quantum reservoir*, which is applied to an initial quantum state representing the input data. The objective is to extract valuable information from it by measuring local operators, yielding the relevant features necessary for predicting the output, which are then fed into a classical machine-learning algorithm, typically a linear model. It has been shown that, for an effective learning of input-output relationships, the quantum reservoir must be a complex enough quantum circuit [7,10,11]. Hence, a careful design of the quantum reservoir is vital to achieve an optimal performance of the QRC model. Moreover, considering the effect of noise in the performance of the reservoir is crucial for the practical applications of quantum reservoir computing, which is carefully studied in a previous work [11]. The majorization principle [22], a statistical concept used to assess the degree of discordance between probability

---

*Contact author: laia.domingo@icmat.es
†Contact author: f.borondo@uam.es
‡Contact author: carlo@tandar.cnea.gov.ar
§Contact author: wisniacki@df.uba.ar

distributions, has emerged as a significant and efficient indicator of complexity for random quantum circuits [22,23], and it has proven to be a compelling indicator of performance in QRC as well [10]. However, given the recent advancements in quantum technologies, there is a pressing need for more powerful complexity methods to understand the physical properties of quantum algorithms that can facilitate the optimal design of large-scale quantum solutions.

In this paper, we present a significant step forward along this line, by delving into a complexity measure known as the Krylov complexity and the associated Lanczos sequence [24,25], which have been proposed for operators [24] and states [26]. These measures are built on robust physical principles, and the Krylov complexity's unique growth behavior provides a precise definition of complexity over large timescales. Moreover, they offer applicability to a broad variety of problems, having proven suitable for analyzing intricate systems in condensed-matter physics [27], quantum field theory [28], and quantum information [29]. In this sense, our analysis of the Krylov complexity paves the road to unlock deeper insights into quantum systems, facilitating the development of superior quantum algorithms for different real-world challenges.

Originally developed to efficiently calculate the exponential of a matrix [30,31], Krylov methods have found widespread use in quantum evolution of states and operators within systems with large Hilbert spaces [32]. These methods involve mapping the system's evolution to a noninteracting tight-binding model within the so-called Krylov space. Such mapping leads to a measure of complexity that has garnered significant attention in recent research [24,25,27,33–41]. The key aspect of this measurement, called K complexity, lies in the concept of spreading of the one-particle wave function over Krylov basis. In fact, it has been demonstrated that, by using this basis, the dispersion of a wave packet is minimized, thereby avoiding ambiguities when defining the complexity associated with quantum evolution. Several authors have extensively considered this measure to study the transition from integrability to chaos in a variety of systems [42–44]. It is important to note that, when applied to operators, the effectiveness of this complexity measure appears to be contingent on the specific operator under consideration [39]. Similarly, in the case of states, it may not yield satisfactory results depending on the initial conditions [45]. However, in the case of state evolution and within the effective tight-binding model, both the Krylov complexity and the statistics of the onsite potentials have shown to be promising robust measures of quantum complexity.

In this paper, we focus on the investigation of the reservoir complexity using Krylov methods to advance in the optimal design for QRC. However, an important challenge arises in the case of reservoirs, as we lack a Hamiltonian description, having instead an evolution operator U(t). To overcome this hurdle, we propose to use an effective Hamiltonian for these reservoir systems, which involves taking the logarithm of the operator U(t). To validate this approach, we first delve into analyzing spin chains as a starting point of our research. By careful examination of the system behavior at different time instances, the Krylov approach is found to effectively quantify the system complexity only when the evolution operator is

used for times smaller than the $t_{1/2}$ time [46]. This specific time is defined as the moment when the K complexity of the system reaches *half* of its asymptotic plateau. Beyond this time, the system exhibits a level of chaoticity that makes it challenging to describe it using conventional methods. We then further proceed with our validation by analyzing the complexity of the standard map, the paradigmatic system extensively studied for both classical and quantum chaos, where, as stated before, the quantum dynamics is governed by an evolution operator, without a Hamiltonian description. Our results demonstrate that the Krylov complexity aligns perfectly with other conventional measures of quantum chaos. The complexity measure derived from Krylov methods provides valuable insights into the quantum reservoir's chaotic dynamics across various temporal scales, especially for times before the onset of significant scrambling effects. This yields more comprehensive information regarding the system's complexity. Additionally, a pivotal objective of our research is to shed light on the relationship between Krylov methods and other well-established measures of complexity, providing a comprehensive understanding of these intriguing quantum systems.

The article is organized as follows: Section II introduces the specifics of QRC and gives an outline of the Krylov method and its application in defining complexity. In Sec. III, we comprehensively demonstrate the efficacy of the Krylov approach in describing complexity based on the evolution operator. We initiate our analysis with spin chains, where the evolution operator is constructed up to a certain time and subsequently transition to discussing the standard map. Finally, we investigate the complexity of reservoirs employed in the QRC model. We conclude the paper with our final remarks.

II. METHODS

A. Quantum reservoir computing

Reservoir computing is a machine-learning framework that harnesses the dynamics of a fixed reservoir, such as a recurrent neural network or a quantum circuit, to process and analyze data, enabling efficient training and prediction tasks. The idea of QRC lies in using a Hilbert space as a high-dimensional embedding of the input data. In this way, the extracted features enhanced by quantum operations are used to feed a classical machine-learning model, which predicts the desired target.

Consider the dataset $\{(x_i, y_i)\}$, where x_i are the input samples and y_i the target outputs. The goal of the machine-learning algorithm is to predict the desired output y_i given an input data sample x_i. In this work, the input data x_i represents the electronic ground state of a molecule, and the output y_i is the first-excited energy of such molecule (see Sec. II A 2). The data samples are encoded as an n-qubit quantum state $|x_i\rangle$. Then, a *random* unitary transformation U implemented by a quantum circuit is applied to extract features from the input data, resulting in the quantum state U $|x_i\rangle$. The operator U is sampled from a carefully selected family of operators, such that U creates enough entanglement to generate useful transformations of the input data while being experimentally feasible. For this reason, the design of the reservoir U is crucial for the optimal performance of the algorithm. In this

work, the quantum reservoirs are designed as random quantum circuits whose gates are chosen from a family containing a finite set of gates. That is, given a family of quantum gates, a quantum circuit is generated by uniformly sampling gates from that family. The depth of the circuit is fixed to depth $=$ 40, and 100 simulations are run for each of the families. We have repeated the experiments with circuits with different number of qubits, $n = 6, 8$, and 10. The K complexity and the statistics of the Lanczos coefficients of the resulting unitary operators U will be compared with the performance of the quantum reservoirs in the machine-learning task presented in Sec. II A 2 for two molecules: LiH, requiring $n = 8$ qubits, and H_2O, requiring $n = 10$ qubits.

After applying U to the initial quantum state, the expected value of single-qubit observables is measured. These observables are Pauli operators $\{X_0, Z_0, \dots, X_j, Z_j, \dots, X_n, Z_n\}$, where X_j, Z_j represent the Pauli operators X, Z applied to qubit j. Notice that, in general, a n-qubit unitary U transforms a simple observable Z (or X) into a linear combination of Pauli operators

$$\text{U}Z\text{U}^\dagger = \sum_k \alpha_k P_k, \tag{1}$$

where $\{P_k\}$ are tensor products of local Pauli operators. Therefore, measuring single Pauli operators of a state which has received a unitary transformation could produce complex nonlinear outputs, which could be represented as a linear combination of exponentially many nonlinear functions [5,20]. As an example, consider a scenario where we encode a two-dimensional classical vector $x = (x_1, x_2), x_1, x_2 \in [0, 1]$ into the quantum state $|x\rangle = (\sqrt{x_1}\,|0\rangle + \sqrt{1 - x_1}\,|1\rangle) \otimes (\sqrt{x_2}\,|0\rangle + \sqrt{1 - x_2}\,|1\rangle)$. When measuring the expectation value of the single-qubit operator Z_1, we observe a linear function of x_1, $\langle Z_1 \rangle = 2x_1 - 1$. However, measuring a correlated operator $Z_1 Z_2$ yields a nonlinear function of x_1 and x_2, $\langle Z_1 Z_2 \rangle = (2x_1 - 1)(2x_2 - 1)$. This correlated operator is achieved by applying a CNOT gate to the input state $|x\rangle$ (where $\text{U} = |0\rangle\langle 0| \otimes \mathbb{I} + |1\rangle\langle 1| \otimes X$), followed by measuring the local Z_2 operator on the resulting state $\text{U}|x\rangle$. Consequently, the unitary transformation U enables the measurement of a nonlinear transformation of the input data.

Finally, the extracted features $\hat{x}_i = (\langle X_0 \rangle, \langle Z_0 \rangle, \dots, \langle X_n \rangle, \langle Z_n \rangle)$, where the expected value is defined with respect to the output state of the quantum reservoir are fed to a classical machine-learning algorithm, usually a linear regression model. Even though more complex models can be used, the quantum reservoir should be able to extract valuable features so that a simple machine-learning model can predict the target y. A linear model with regularization, called ridge regression, is enough to learn the output. A Ridge regression consists of learning the optimal parameters W that minimizes the following expression:

$$\text{MSE}_r(\hat{y}, y) = \frac{1}{t} \sum_{t=1}^{T} [(y(t) - W\hat{x}(t)]^2 + \gamma\,||W||^2, \tag{2}$$

where γ is the regularization parameter and W are the linear coefficients and $||\cdot||^2$ is the L^2 norm. This loss function prevents the algorithm from learning large coefficients W, which usually leads to unstable training and poor generalization capacity. γ is a hyperparameter which needs to be tuned depending on the problem at hand. When γ is too large, the model will learn very small values of W, which leads to predicting constant values. On the other hand, if γ is too small the chances of overfitting increase.

1. Families of quantum reservoirs

The design of the quantum reservoir is crucial for the performance of the algorithm. For this reason, seven *families* of quantum circuits are studied. For a given family, the quantum circuit is built by adding a fixed number of random quantum gates from such family. For each family, 100 simulations are carried out.

The seven families of quantum reservoirs can be ordered in terms of complexity according to the majorization principle [23], which in turn corresponds to different performances in QRC [10]. In this study, we demonstrate that the distinction in complexity can also be quantified using the Krylov evolution. As a result, Krylov measures offer excellent means to identify optimal families of random quantum circuits for machine-learning tasks. This approach provides a more precise and quantitative method for comprehending the variations between various quantum reservoir designs, enabling the formulation of practical guidelines for efficient quantum algorithm implementations. Additionally, it bridges the gap between quantum machine-learning designs and quantum complexity theory, opening up new possibilities for advancements in quantum machine-learning research.

The seven families considered are the following: The first three circuits are constructed from a few generators: G1 $=$ {CNOT, H, X}, G2 $=$ {CNOT, H, S}, and G3 $=$ {CNOT, H, T}, where CNOT is the controlled-NOT gate, H stands for Hadamard, and S and T are $\pi/4$ and $\pi/8$ phase gates, respectively. The circuits constructed from G2 generate the Clifford group [47], and G1 generate a subgroup of Clifford [48]. Therefore, both G1 and G2 are nonuniversal and classically simulatable. On the other hand, G3 is universal and thus approximates the full unitary group U(N) to arbitrary precision. The fourth family is composed of matchgates (MGs), which are two-qubit gates formed from two one-qubit gates, A and B, with the same determinant. Matchgates circuits are also universal (except when acting on nearest-neighbor lines only) [49,50]. The last families of gates are diagonal in the computational basis and are divided into three families: D_2, D_3, and D_n. Here, D_2 gates are applied to pairs of qubits, D_3 gates are applied to three qubits, and D_n gates are applied to all the qubits. Diagonal circuits cannot perform universal computation but they are not always classically simulatable [51]. For more details about these families of quantum reservoirs see Appendix A.

2. Quantum machine-learning task

To assess the performance of the different quantum reservoirs, a machine-learning task needs to be defined. In this work, the task consists of predicting the first-excited electronic energy E_1 using only the associated ground state $|\psi_0\rangle_R$ with energy E_0 for the LiH and H_2O molecules. The ground states $|\psi_0\rangle_R$ for such Hamiltonians are calculated by exact diagonalization for different configuration ranges:

$R_{\text{LiH}} \in [0.5, 3.5]$ a.u. (atomic units), $R_{\text{OH}} \in [0.5, 1.5]$ a.u., and $\phi_{\text{HOH}} = 104.45°$. The details of the ground-state calculation are given in Ref. [10]. Notice that, in order to use as few qubits as possible, we remove the spin-orbitals which are very likely to be either occupied or virtual in all Slater determinants in the wave function [52]. In this way, the electronic Hamiltonian is effectively mapped to the qubit space by using the Jordan-Wigner transformation [53]. The ground state of the molecules is described using $n = 8$ qubits for LiH and $n = 10$ qubits for H_2O. The datasets $\{|\psi_0\rangle_R, E_1(R)\}_R$ is split into training and test sets, where the test set contains the 30% of the data $R_{\text{LiH}} \in [1.1, 2.0]$ a.u. and $R_{\text{OH}} \in [1.05, 1.35]$ a.u. and it is chosen so that the reservoir has to extrapolate to unseen data. The performance of the seven families of quantum reservoirs will be compared with the Krylov evolution.

B. The Krylov approach to complexity

The Krylov method is a numerical technique originally designed to approximate the action of a matrix or operator on a vector, without explicitly calculating the full matrix elements [30,31]. It is particularly useful when dealing with large matrices or operators, which are common in quantum mechanics, especially in the context of solving the time-dependent Schrödinger equation, Heisenberg evolution of operators, or eigenvalue problems [30,32,54–59]. Notably, it has been recently used to determine the complexity of quantum evolution for both operators and states [24–26]. In this work, we focus on the second case, i.e., states.

Let us consider a state $|\psi\rangle$ in a complex Hilbert space $\mathcal{H}$ with dimensionality N, i.e., $\mathcal{H} = \mathbb{C}^N$. This state evolves under the influence of a time-independent Hamiltonian denoted by $H \in \text{End}(\mathcal{H})$. We introduce the D-dimensional Krylov subspace, denoted $\mathcal{K}_D$,

$$\mathcal{K}_D = \text{span}\{|\psi\rangle, H|\psi\rangle, \ldots, H^{D-1}|\psi\rangle\}. \quad (3)$$

To ensure generality, we assume that the state $|\psi\rangle$ and the Hamiltonian H do not share any symmetries, meaning $\mathcal{K}_N = \mathcal{H}$. When there are shared symmetries, the time evolution is constrained within their respective subspaces. Consequently, the problem should be redefined to operate solely within that subspace.

The Krylov method endeavors to approximate the time-evolved state $|\psi(t)\rangle$ using the most optimal element from the set $\mathcal{K}_D$. To accomplish this, we create a set of orthonormal basis vectors, denoted as $B_D = \{|v_0\rangle \equiv |\psi\rangle, \ldots, |v_{D-1}\rangle\}$, for the Krylov subspace. Usually, the basis is created using Lanczos's algorithm, which is a modified version of the Gram-Schmidt procedure. Lanczos's algorithm leverages the fact that orthonormalization is only required for the last two vectors in the basis. In order for the Krylov subspace to fully encompass the entire evolution at all times, it must span the entire Hilbert space, meaning that $D = N$, where D represents the dimension of the Hilbert space. By following this approach, the Hamiltonian is transformed into its tridiagonal form,

$$H|v_k\rangle = a_n|v_k\rangle + b_{k+1}|v_{k+1}\rangle + b_k|v_{k-1}\rangle, \quad (4)$$

where a_k and b_k are values that define the Lanczos sequences. This observation leads us to interpret the system on the Krylov

basis, as a one-dimensional (1-D) noninteracting tight-binding model. An initial state localized at one end of this effective chain evolves under the influence of the onsite potentials a_k and hopping amplitudes b_k at the nth site—causing the excitation to propagate and populate the rest of the lattice.

By expressing the evolved state $|\psi(t)\rangle$ in this Krylov basis, we have

$$|\psi(t)\rangle = \sum_{k=0}^{D-1} \psi_k(t)|v_k\rangle. \quad (5)$$

The coefficients $\psi_k(t)$ can be obtained by solving the Schrödinger equation,

$$i\,\dot{\psi}_k(t) = a_k\psi_k(t) + b_k\psi_{k-1}(t) + b_{k+1}\psi_{k+1}(t). \quad (6)$$

From this formalism, the concept of Krylov complexity denoted by $C_{\mathcal{K}}^{\psi}(t)$ arises, which represents the average position

$$C_{\mathcal{K}}^{\psi}(t) = \sum_{k=0}^{D-1} k|\psi_k(t)|^2. \quad (7)$$

This complexity measure can be understood as the average dimension of the Krylov subspace needed to accurately represent the evolution of the initial state over time.

In recent studies [42–44], the potential of using Krylov complexity as a reliable measure to assess the transition from integrability to chaos has been explored. This investigation has been conducted in various systems, including those with and without semiclassical limits. The results indicate that both the complexity and variance of the Lanczos coefficients provide an excellent description of this transition when considering Krylov evolution for states.

III. RESULTS

In this section, we analyze the performance of quantum reservoirs using the Krylov approach to complexity.

In the realm of QRC, random quantum circuits are represented by a unitary evolution operator U, which creates a quantum-enhanced representation of the input data. A problem arises here; although the Krylov method is typically well defined for studying quantum systems when described by a Hamiltonian operator, there is no satisfactory adaptation for the case of unitary operators. This severe limitation needs to be addressed beforehand to make it possible to study the Krylov complexity for quantum reservoirs. To this end, we introduce in Sec. III A a suitable method to analyze the Krylov complexity with quantum unitaries, which is then validated by showing that it can accurately reproduce the properties of two benchmark quantum systems with chaotic dynamics: the longitudinal-transverse field Ising model and the standard map.

A. Krylov complexity for evolution operators

The method that we propose to use is simple. Given an evolution operator U, a corresponding effective Hamiltonian H_{eff} is calculated as

$$H_{\text{eff}} = -i \ln \text{U}. \quad (8)$$

We show that this choice allows us to use the above method to characterize the K complexity of U. The operator H_{eff} is then used to calculate the Lanczos coefficients and Krylov complexity for an initial quantum state $|\psi\rangle$.

To validate this ansatz, we first apply the proposed method to the longitudinal-transverse field Ising model, with nearest-neighbor interactions in the z direction, and a transverse magnetic field in the (x, z) plane. The corresponding Hamiltonian is then given by

$$H = \sum_{k=1}^{n} \left(h_x \sigma_k^x + h_z \sigma_k^z \right) - J \sum_{k=1}^{n-1} \sigma_k^z \sigma_{k+1}^z, \quad (9)$$

where n is the number of spin $-1/2$ sites in the chain, σ_k^j is the Pauli operator at site $k = 1, 2, \ldots, n$ in the x, y, and z directions, h_x and h_z are the components of the magnetic field, and J is the nearest-neighbor coupling. To expand an operator in the Krylov space, it is necessary to work in a symmetry subspace. Our system is invariant under reflection with respect to the center of the chain. In this work, we always operate in the positive-parity subspace and fix $\hbar = 1$ and the coefficients $h_x = J = 1$, so that the energy h_z is measured in units of J. Hamiltonian (9) is integrable for $h_z = 0$ and for $h_z \gtrsim 3$, while it exhibits a quantum chaotic behavior for intermediate values of h_z.

We next construct the evolution operator $U = e^{iHT}$ for our Hamiltonian. In this case, the unitary is also normalized to the chosen time T, to recover the scale of the original Hamiltonian. Finally, the chaotic properties of H_{eff} associated with the Ising model are computed for three different values of the characteristic time, which all have units of J^{-1}. The longest one is taken as the Heisenberg time,

$$t_H = \frac{2\pi}{\rho_E}, \quad (10)$$

where ρ_E represents the mean density of states around energy E. The second time is the $t_{1/2}$ time, defined as the time it takes to reach half the value of the saturation of the K complexity calculated using H of Eq. (9). Figure 1 shows the scaling of the $t_{1/2}$ time with the number of spins of the quantum system, which increases cubically with n. This power-law behavior is characteristic of integrable or mixed systems than chaotic [60], which requires a more detailed study that we will do in the future. A representation of how the $t_{1/2}$ time is defined is shown in the inset. Finally, a third time is chosen, corresponding to a short period of time $t_{1/2}/25$.

With these three timescales, we study the chaotic dynamics of the Ising Hamiltonian for different values of h_z for a system with $n = 10$ spins. The results are displayed in Fig. 2. There, the black curve shows the mean value of the distribution of the ratio of consecutive level spacings $\bar{r}$ calculated with the actual Hamiltonian in Eq. (9) [61–63], which indicates the regular or chaotic character of the system according to criteria of random matrix theory [64]. This curve clearly shows a very sudden phase transition from an integrable system for $h_z \approx 0$ to a chaotic system for $h_z \approx 1$, and gradually back to an integrable system for $h_z \gtrsim 3$. On the other hand, the color curves show the values of $\bar{r}$ calculated with the effective Hamiltonian H_{eff} for the three characteristic times using Eq. (8). As can be seen, when the timescale is short, i.e., $t_{1/2}/25$, H_{eff} correctly
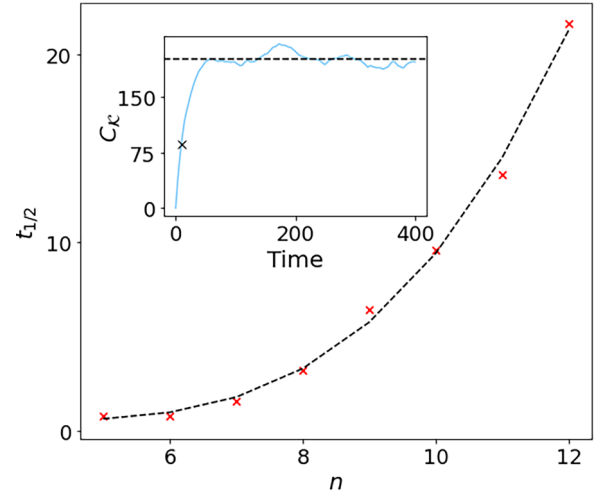

FIG. 1. Scaling of the $t_{1/2}$ with the number of quantum spins (n) in the Ising model (9). The inset illustrates the calculation of the $t_{1/2}$ time, defined as the duration required for the K complexity $C_{\mathcal{K}}$, as defined in Eq. (7) to reach half of the average value at the plateau for a system of size $n = 10$.

reproduces the behavior of $\bar{r}$. However, when the characteristic time increases, the resulting effective Hamiltonian loses the phase transition, becoming integrable for all values of h_z.

To complete our study, we show in Fig. 3 the mean K complexity, $\overline{C_{\mathcal{K}}}$, averaged over multiple initial quantum states,

$$\overline{C_{\mathcal{K}}} = \frac{1}{m} \sum_{i=0}^{m-1} \int_{T_1}^{T_2} C_{\mathcal{K}}^{\psi_i}(t) dt, \quad (11)$$
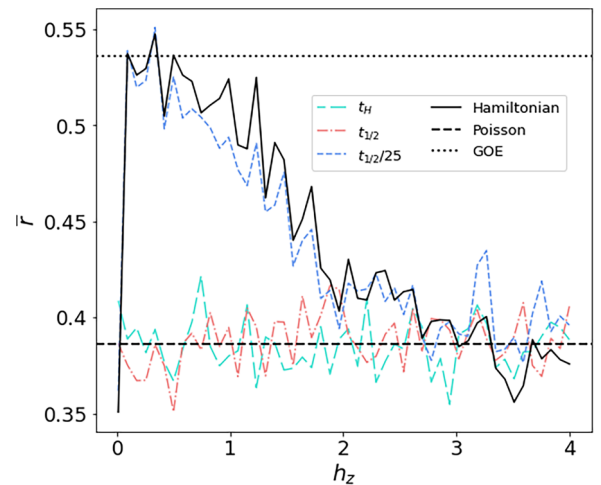

FIG. 2. Mean value of the distribution of the ratio of consecutive level spacings $\bar{r}$ for the Ising model of Eq. (9) as a function of the coupling constant h_z, measured in units of J. The values $\bar{r} \approx 0.386$ (horizontal dashed line) and $\bar{r} \approx 0.536$ (horizontal dotted line) corresponds to a regular and a chaotic system, respectively. The Hamiltonian has been constructed from the unitary evolution operator for three different times: the Heisenberg time t_H, the $t_{1/2}$ time, and a shorter period of time $t_{1/2}/25$, all measured in units J^{-1}. The black curves represent the statistics obtained with the Ising-model Hamiltonian.
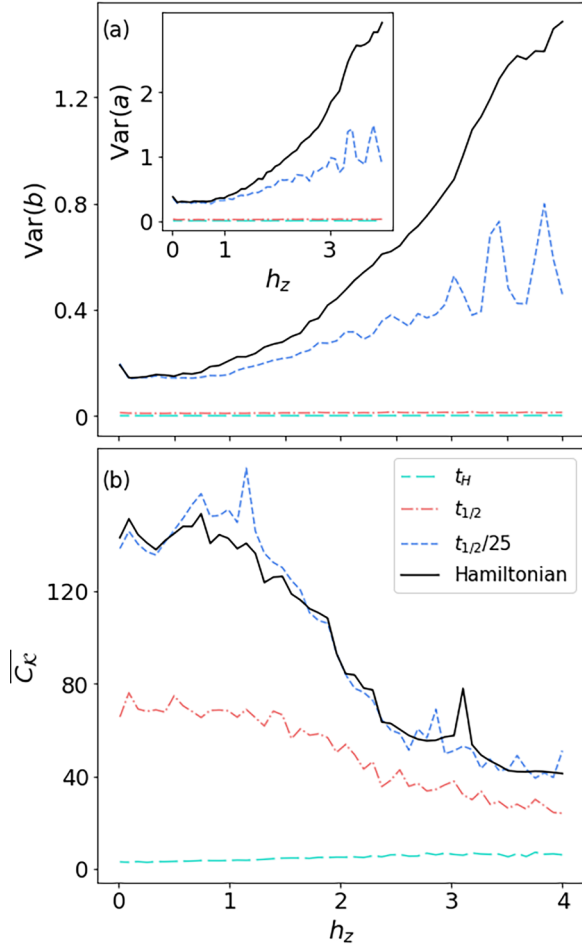
FIG. 3. (a) Variance of the Lanczos coefficients a and b for the Ising model with $n = 10$ spins, as a function of h_z, measured in units of J. (b) Mean K complexity $\overline{C_\mathcal{K}}$ as a function of h_z. The three times used are the same as in Fig. 2.

where the initial states $|\psi_i\rangle$ are chosen to be eigenvalues of the Ising Hamiltonian in Eq. (9) and T_1 is chosen so that the system has arrived at saturation and T_2 is the final time for our simulations. Figure 3 also shows the variance of the Lanczos coefficients a and b for the same three timescales considered before. The Krylov complexity has been computed using several initial states $|\psi\rangle$ [see Eq. (3)], that are eigenstates of H in the integrable regime ($h_z > 5$). Let us remark that the choice of the initial states is vital to accurately capture the evolution of the K complexity with h_z [45]. The results in Fig. 3(a) shows that the variance of a and b increases with h_z for the true Hamiltonian (black curve). However, as the time period becomes longer, the variance of such coefficients increases in a slower fashion (colored curves). In fact, in the limit $t = t_H$ the variance of the coefficients is basically constant. Complementarily, Fig. 3(b) shows $\overline{C_\mathcal{K}}$ at the $t_{1/2}$ time for the different timescales, from which it can be concluded that, while for $t = t_{1/2}/25$ the dynamics of $\overline{C_\mathcal{K}}$ is correctly reproduced, the pattern is completely lost at $t = t_H$, and for $t = t_{1/2}$ it exhibits an intermediate dynamics.

The previous results show that as long as the time of the evolution operator is small enough, the effective Hamiltonian,
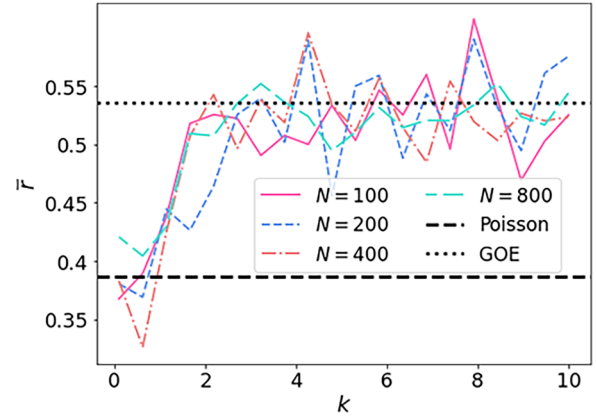

FIG. 4. Variation of $\overline{r}$ as a function of the chaos parameter k for the standard map.

introduced by us in Eq. (8), is able correctly reproduce the chaotic dynamics of the system ($\overline{r}$), as well as the K complexity ($\overline{C_\mathcal{K}}$). Notably, the computational time and resources required to apply this method to large-scale systems can be substantially reduced by considering *only* the first few coefficients of the Lanczos sequence. As it is shown in Appendix B, the coefficients still allow for an accurate reproduction of the Krylov statistics and complexity.

To further confirm our previous conclusions, we consider a second benchmark system, with different mathematical characteristics. This system is the (quantum) standard map, a quantum-mechanical version of the classical standard map, which describes the dynamics of a periodically kicked rotor system on a torus. The associated torus structure gives rise to periodicity in both position and momentum. When quantized, this periodicity leads to a discrete Hilbert space with a dimension of N, and Planck constant denoted $h = 1/(2\pi N)$.

Mathematically, the standard map is defined by a unitary operator U such that

$$|\psi\rangle \longrightarrow \mathrm{U}\,|\psi\rangle = e^{-i\,\frac{\hat{p}^2}{2}}\,e^{-i\,k\cos(2\pi\hat{x})}\,|\psi\rangle, \qquad (12)$$

where $\hat{x}$ is the position operator, $\hat{p}$ is the momentum operator, and k is the chaos parameter. For small values of k, the level spacing statistics ($\overline{r}$) is described by the Poisson law, and by the Wigner-Dyson law of the random matrix theory for large values of k [42]. This behavior is depicted in Fig. 4, which shows the variation of $\overline{r}$ with the parameter k for different sizes of the Hilbert space. As can be seen, the evolution of $\overline{r}$ is qualitatively equivalent for all different system sizes considered.

Similarly to what we did before with the Ising model, for which the system Hamiltonian was known, we have obtained the mean complexity $\overline{C_\mathcal{K}}$ and variance of the Lanczos coefficients with the effective Hamiltonian H_eff in Eq. (8). The results, displayed in Fig. 5, show that also in this case the Krylov statistics correctly reproduce the quantum chaotic behavior of the system. In particular, Fig. 5(a) shows that the variance of the Lanczos coefficients decreases as k increases, in accordance with the behavior of the mean level spacing $\overline{r}$ [39,42]. Moreover, Fig. 5(b) shows that the mean and variance of the K complexity also increase (decrease) with k, result
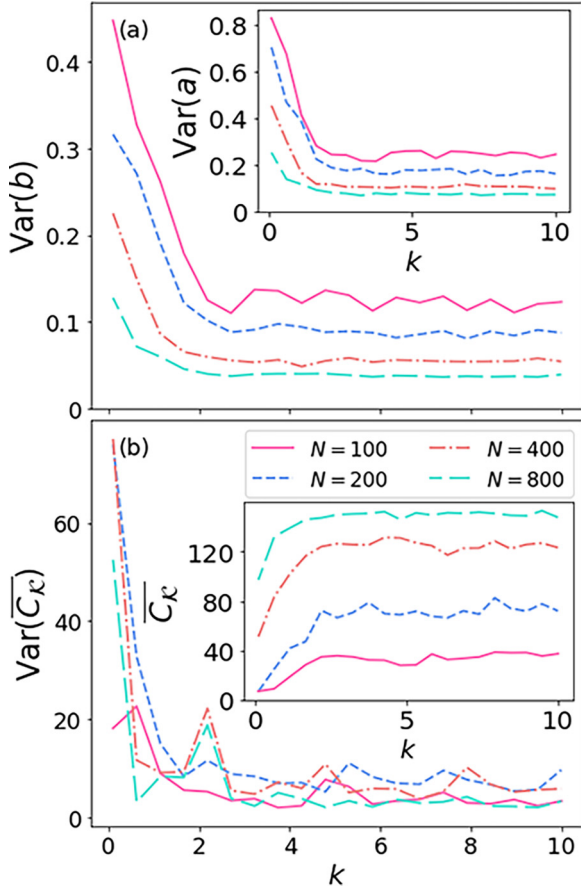
FIG. 5. Same as Fig. 3 for the standard map with Hilbert-space sizes $N = 100, 200, 400,$ and 800.

FIG. 6. Same as Fig. 3 for the seven families of quantum reservoirs for $n = 10, 8,$ and 6. $\overline{C_\mathcal{K}}$ and $\mathrm{Var}(\overline{C_\mathcal{K}})$ have been normalized with the dimension of the Hilbert space for better visualization.

which also reproduces the integrable-chaotic transition taking place in the system with k. Here, variances are calculated over the 100 simulations varying the initial state $|\psi\rangle$ of the system [see Eq. (3)], which are all chosen to be eigenstates of the standard map in the integrable region with $k = 0.01$.

In summary, we can state that our results reflect that the Krylov dynamics obtained with the effective Hamiltonian correctly captures the complexity and chaotic properties of a quantum map. This confirms the fact that our construction of H_{eff} is a valid method to compute the K complexity of a unitary operator, which will be next used to calculate the Krylov statistics for the title case of multiple quantum reservoirs.

B. Krylov complexity for quantum reservoirs

Once our method described in Sec. III A has been validated, we proceed to discuss the results for the chaotic and Krylov statistics of seven families of random quantum circuits, which often serve as quantum reservoirs, and compare them with their performance in QRC (see Sec. II A 2).

We begin by analyzing the statistics of the Lanczos coefficients, together with the mean and variance of the K complexity for the seven families of quantum reservoirs. The corresponding results are presented in Fig. 6. In particular, Fig. 6(a) depicts the variance of the Lanczos coefficients a and b, showing that the families achieving better performance [lower mean squared error (MSE)] are also those with smaller
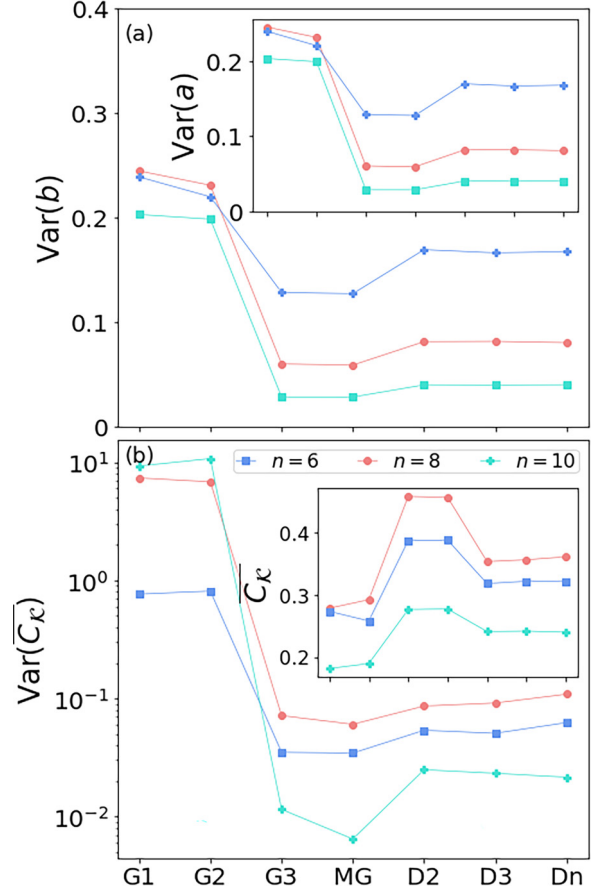
variance in a and b. The variances here have been calculated over 100 simulations performed for each family. The initial state $|\psi\rangle$ is here chosen randomly from the computational basis. Moreover, Fig. 6(b) also indicates the existence of a significant correlation in the mean and variance of the K complexity, with the better-performing reservoirs having lower $\mathrm{Var}(\overline{C_\mathcal{K}})$ and higher $\overline{C_\mathcal{K}}$. Therefore, these results clearly show that the Krylov statistics are an excellent choice for designing optimal quantum reservoirs, which present high performance for quantum machine-learning tasks.

One final point is worth discussing here. In Refs. [10,11], we studied the distribution of the unitary operators generated by the seven families of quantum reservoirs in the Pauli space, which is the space of quantum operators. Using a simple toy model of two qubits, we demonstrated that the less complex families of reservoirs, G1 and G2, only span a small subspace of the operator space. On the other hand, the more complex families, such as G3 and MG, uniformly sample the entire operator space, resulting in improved performance in QRC. Now, the Krylov approach to complexity further clarifies and allows a better understanding of this result. Indeed, the K complexity measures the average dimension of the Krylov subspace required to represent the evolution of an initial state over time, described by the unitary operator sampled from any of the quantum reservoir families. Therefore, only the families
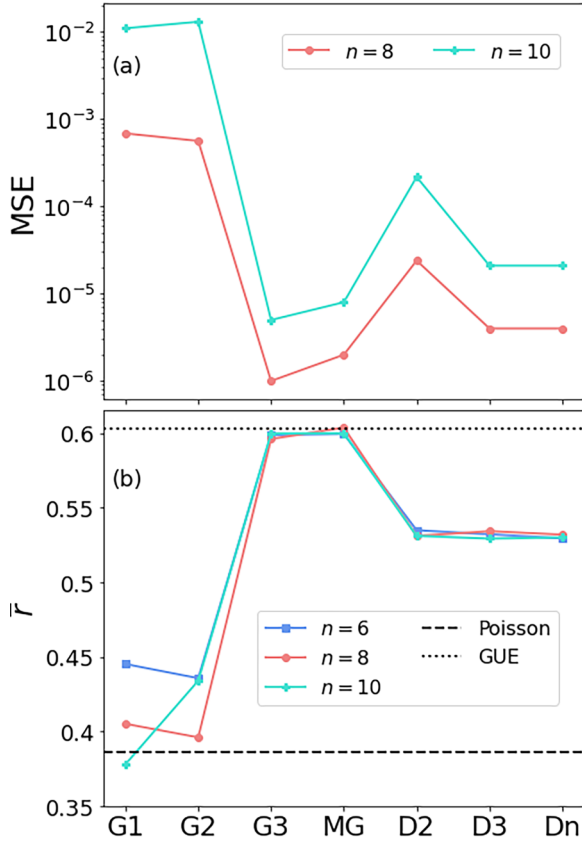
FIG. 7. (a) Mean squared error (MSE), obtained with the quantum reservoir computing algorithm for the seven families of quantum reservoirs and the two molecules: LiH ($n = 8$) and H_2O ($n = 10$). The MSE has units of energy squared, which is expressed in atomic units. (b) Variation of $\bar{r}$ for the different families of quantum reservoirs with sizes $n = 6$, 8, and 10.

able to generate the whole set of quantum operators will be able to span larger Krylov subspaces, then giving rise to higher values of $\overline{C_\mathcal{K}}$. On the contrary, families that only produce nonuniversal, limited sets of quantum operators will result in low-dimensional Krylov spaces, leading to lower complexity values.

This is clearly seen in the results of Fig. 7, which compares the mean squared error (MSE) of the predictions in the machine-learning tasks [Fig. 7(a)] reported in Ref. [10], with the mean energy-level spacing, $\bar{r}$, for the seven families of quantum reservoirs [Fig. 7(b)] obtained here. The results show that there is a strong correlation between the quantum chaotic behavior of the families of quantum circuits and the performance in QRC. Actually, the families with higher values $\bar{r}$, such as the G3 and MG, are also those providing better performance as quantum reservoirs. On the contrary, G1 and G2 are the families with worse performance, which also present lower values of $\bar{r}$. Finally, the diagonal circuits D_2, D_3, and D_N provide intermediate results both in terms of MSE and $\bar{r}$.

IV. CONCLUSIONS

In the realm of the rapidly progressing field of developing quantum methods for NISQ devices, which is aimed at

surpassing classical approaches using the currently available quantum computers, QRC algorithm has emerged as a standout approach. This algorithm harnesses the inherent properties and dynamics of a quantum system, referred to as the quantum reservoir, to discover hidden patterns within the input data crucial to perform optimal machine-learning tasks. Indeed, the design of the quantum reservoir is of uttermost importance for the successful implementation of the algorithm. In this respect, it was recently proven that the complexity of the quantum reservoir, measured by the majorization criterion [23], is an excellent indicator of performance in machine-learning tasks [10,11].

Building upon this knowledge, the present work expands the understanding by providing a quantitative and precise method to assess the performance of quantum reservoirs, employing the Krylov approach to complexity. The Krylov complexity relies on robust physical principles, and its distinctive growth pattern offers a precise characterization of complexity across multiple temporal scales. This technique entails representing the system's evolution through a mapping onto a noninteracting tight-binding model within the Krylov space. The K complexity is derived by spreading a one-particle wave-function across the Krylov basis. Utilizing this basis minimizes the dispersion of a wave packet, thus circumventing uncertainties in defining complexity associated with quantum evolution and providing valuable insights into the system's chaotic nature. To evaluate the K complexity for quantum reservoirs, we first had to develop a technique able to calculate the Krylov evolution for quantum unitary operators. Through this approach, we successfully reproduced the chaotic phase transition of two quantum systems, namely, the longitudinal-transverse-field Ising Hamiltonian and the standard map, validating our ansatz of Eq. (8).

Subsequently, we demonstrated that Krylov statistics, including the mean K complexity at saturation $\overline{C_\mathcal{K}}$ and its variance $\mathrm{Var}(\overline{C_\mathcal{K}})$, along with the variance of the Lanczos coefficients, exhibit a strong correlation with the performance of quantum reservoirs measured as the mean squared error of the predicted electronic energies of multiple molecules. Consequently, the Krylov evolution emerges as an efficient and precise tool for estimating the performance of QRC. Furthermore, the Krylov approach has the potential to evaluate the complexity of additional quantum substrates that serve as quantum reservoirs, including bosonic [65] and fermionic systems [66], as well as optical networks, thus expanding the comprehension of complexity within QRC to a wider range of contexts. These findings hold immense promise for designing optimal quantum algorithms involving random quantum systems, facilitating successful implementations of quantum machine-learning methods.

The underlying code for this study is available in the GitHub repository and can be accessed online [67].

APPENDIX A: FAMILIES OF QUANTUM RESERVOIRS

The seven families of quantum reservoirs considered in this work are the following:

(1) G1: The quantum circuit is constructed from the generator G1 = {CNOT, H, X}, where CNOT is the controlled-NOT gate, H stands for a Hadamard gate, and X is the NOT gate. The set G1 generates a subgroup of Clifford [48] group and thus is nonuniversal and classically simulatable.

(2) G2: The quantum circuit is constructed from the generator G2 = {CNOT, H, S}, with S being the $\pi/4$ phase gate. The circuits constructed from G2 generate the whole Clifford group [47], so they are nonuniversal and classically simulatable but more complex than G1 circuits.

(3) G3: The quantum circuit is constructed from the generator G3 = {CNOT, H, T}, where T is the $\pi/8$ phase gate. G3 is universal and thus approximates the full unitary group $U(N)$ to arbitrary precision.

(4) Matchgates (MGs): Two-qubit gates formed by two one-qubit gates A and B with the same determinant. A acts on the subspace spanned by $|00\rangle$ and $|11\rangle$, while B acts on the subspace spanned by $|01\rangle$ and $|10\rangle$. A and B are randomly sampled from the unitary group $U(2)$:

$$G(A, B) = \begin{pmatrix} a_1 & 0 & 0 & a_2 \\ 0 & b_1 & b_2 & 0 \\ 0 & b_3 & b_4 & 0 \\ a_3 & 0 & 0 & a_4 \end{pmatrix}, \quad |A| = |B|. \quad \text{(A1)}$$

Matchgates circuits are also universal (except when acting only on nearest-neighboring lines) [49,50].

(5) Diagonal-gate circuits ($\mathbf{D_2}$, $\mathbf{D_3}$, $\mathbf{D_n}$): The last families of gates are diagonal in the computational basis. The diagonal gates are separated into three families: D_2, D_3, and D_n. Here, D_2 gates are applied to pairs of qubits, D_3 gates are applied to three qubits, and D_n gates are applied to all qubits:

$$D_k(\phi_1, \ldots, \phi_{2^k}) = \begin{pmatrix} e^{i\phi_1} & 0 & \cdots & 0 \\ 0 & e^{i\phi_2} & \cdots & 0 \\ \vdots & \vdots & \ddots & \vdots \\ 0 & 0 & \cdots & e^{i\phi_{2^k}} \end{pmatrix}, \quad \text{(A2)}$$

for $k \in \{2, 3, n\}$ and with ϕ_i chosen uniformly from $[0, 2\pi) \; \forall \; i$. The gates are applied on all combinations of k (out of n) qubits, the ordering being random. At the beginning and at the end of the circuit (after the initialization of the state), Hadamard gates are applied to all qubits. As diagonal gates commute, they can be applied simultaneously. Diagonal circuits cannot perform universal computation but they are not always classically simulatable [51]. As opposed to the other families of circuits, which can be of arbitrary depth, the diagonal D_2, D_3, and D_n families contain a fixed number of gates, being those $\binom{n}{2}$, $\binom{n}{3}$, and 1 gates, respectively.
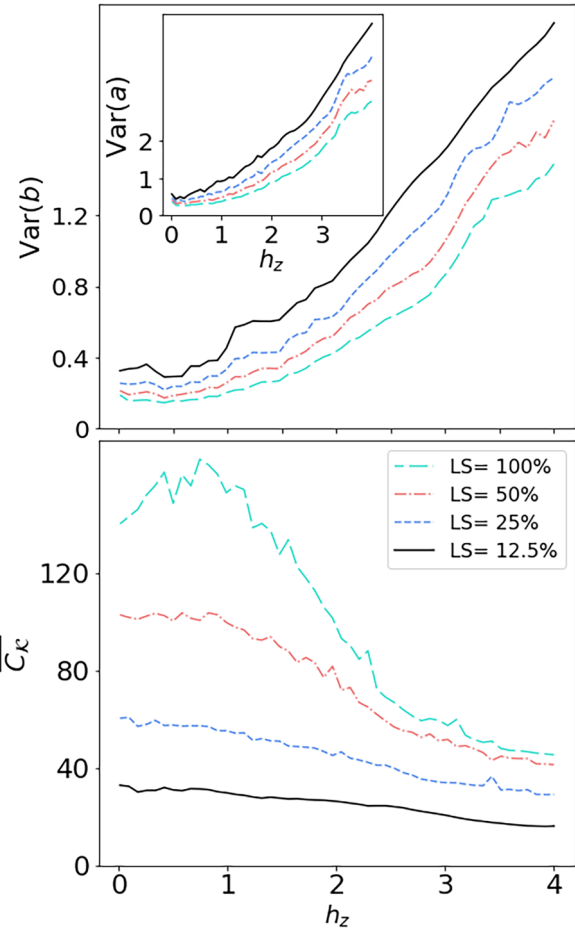

FIG. 8. (top) Variance of the Lanczos coefficients a and b for the Ising model with $n = 10$ spins, as a function of h_z in units of J (bottom). Mean K complexity ($\overline{C_\mathcal{K}}$) as a function of h_z. The size of the Lanczos sequence (LS) is reduced to 100%, 50%, 25%, and 12.5%.

APPENDIX B: KRYLOV APPROACH WITH REDUCED LANCZOS COEFFICIENTS

In this Appendix, we study the performance of the Krylov approach when considering only a simplified subset of coefficients from the complete Lanczos sequence. Rather than calculating the Krylov complexity and statistics using all coefficients a and b, we perform the calculations here using only a fraction of these coefficients while disregarding the tail end of the sequence. The percentage of the sequence of the Lanczos coefficients used for the calculations will be called the Lanczos sequence (LS) from now on.

Figure 8 (top panel) illustrates the variance of a and b, while Fig. 8 (bottom panel) shows the mean complexity $\overline{C_\mathcal{K}}$ with respect to different initial conditions for the Ising model with $n = 10$ spins. The colored lines in the graphs represent the obtained statistics using all Lanczos coefficients (green) and also when using only a fraction of them, with LS = 50% (red), 25% (blue), and 12.5% (black). As can be seen in the bottom panel of Fig. 8, the transition of the K complexity is accurately reproduced when using all Lanczos coefficients and also fairly well reproduced when only 50% of the

coefficients are included. On the contrary, the K complexity phase transition is completely lost when using only a small fraction of coefficients, for example, 12.5%. On the other hand (Fig. 8, top panel), the evolution of the variance of the Lanczos coefficients is well reproduced even when using very small fractions of the Lanczos sequence, as it consistently exhibits a growing behavior with respect to h_z. More interestingly, the variance obtained from smaller fractions of coefficients actually shows higher variances than those obtained from the entire set of coefficients. These findings indicate that when studying the dynamics of Lanczos coefficients, one can focus solely on the first few values and still achieve accurate results, leading to a significant reduction in the computational complexity of the method. As for the K complexity, its evolution is reasonably replicated when using smaller sets of coefficients, but its trend becomes completely lost when considering only the initial few values.

Finally, the same trends are observed when studying the quantum standard map for $N = 400$, as depicted in Fig. 9. The behavior of the variance of the Lanczos coefficients is well-reproduced even for smaller sets of coefficients, with as little as 12.5% of them being sufficient. Moreover, thcce K complexity is also well-reproduced when using only 50% of the coefficients, but its dynamics are lost when using 25% and 12.5% of the coefficients. These results highlight the computational efficiency of the Krylov approach, as significantly reducing the size of the Lanczos coefficients still allows for an accurate reproduction of the Krylov statistics and complexity. Consequently, employing only the first coefficients of the Lanczos sequence can substantially reduce the computational time and resources required to apply this method to large-scale systems.
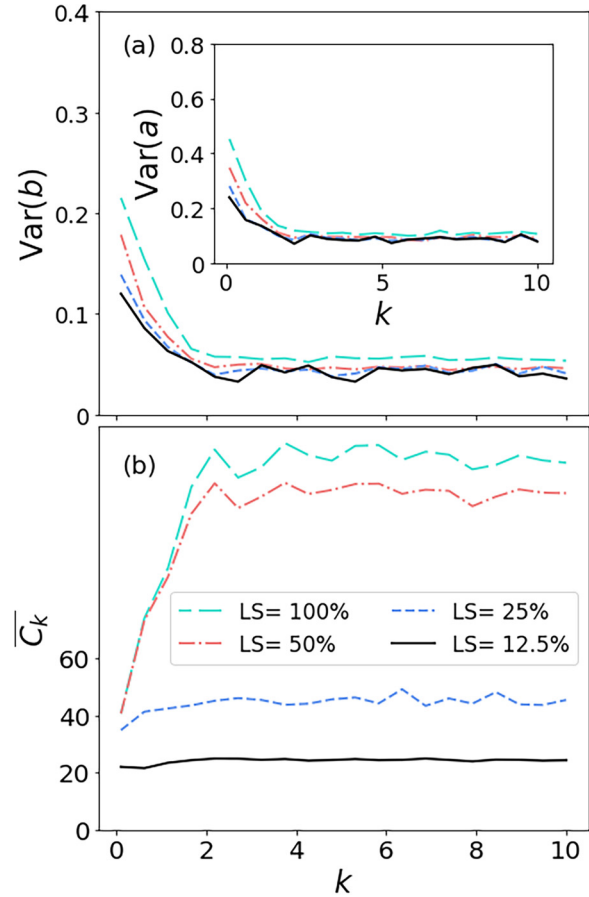

FIG. 9. Same as Fig. 8 but for the quantum standard map with $N = 400$.

[1] P. W. Shor, SIAM J. Comput. **26**, 1484 (1997).

[2] L. K. Grover, in *Proceedings of the Twenty-Eighth Annual ACM Symposium on Theory of Computing: STOC '96, Philadelphia, Pennsylvania* (Association for Computing Machinery, New York, NY, USA, 1996), pp. 212–219.

[3] K. Bharti, A. Cervera-Lierta, T. H. Kyaw, T. Haug, S. Alperin-Lea, A. Anand, M. Degroote, H. Heimonen, J. S. Kottmann, T. Menke, W.-K. Mok, S. Sim, L. C. Kwek, and A. Aspuru-Guzik, Rev. Mod. Phys. **94**, 015004 (2022).

[4] J. Preskill, Quantum **2**, 79 (2018).

[5] K. Fujii and K. Nakajima, Quantum reservoir computing: A reservoir approach toward quantum machine learning on near-term quantum devices, in *Reservoir Computing: Theory, Physical Implementations, and Applications*, edited by K. Nakajima and I. Fischer (Springer Singapore, Singapore, 2021), pp. 423–450.

[6] S. Ghosh, A. Opala, M. Matuszewski, T. Paterek, and T. C. H. Liew, npj Quantum Inf. **5**, 35 (2019).

[7] R. Martínez-Peña, G. L. Giorgi, J. Nokkala, M. C. Soriano, and R. Zambrini, Phys. Rev. Lett. **127**, 100502 (2021).

[8] P. Mujal, R. Martínez-Peña, J. Nokkala, J. García-Beni, G. L. Giorgi, M. C. Soriano, and R. Zambrini, Adv. Quantum Technol. **4**, 2100027 (2021).

[9] A. Kutvonen, K. Fujii, and T. Sagawa, Sci. Rep. **10**, 14687 (2020).

[10] L. Domingo, G. G. Carlo, and F. Borondo, Phys. Rev. E **106**, L043301 (2022).

[11] L. Domingo, G. Carlo, and F. Borondo, Sci. Rep. **13**, 8790 (2023).

[12] H. Jaeger, German National Research Center for Information Technology GMD Technical Report No. 148 (2001).

[13] G. Tanaka, T. Yamane, J. B. Héroux, R. Nakane, N. Kanazawa, S. Takeda, H. Numata, D. Nakano, and A. Hirose, Neural Netw. **115**, 100 (2019).

[14] S. Ghosh, K. Nakajima, T. Krisnanda, K. Fujii, and T. Liew, Adv. Quantum Technol. **4**, 2100053 (2021).

[15] P. Zapletal, A. Nunnenkamp, and M. Brunelli, PRX Quantum **3**, 010301 (2022).

[16] H. Kawai and Y. Nakagawa, Mach. Learn.: Sci. Technol. **1**, 045027 (2020).

[17] P. Mujal, R. Martínez-Peña, G. L. Giorgi, M. C. Soriano, and R. Zambrini, npj Quantum Inf. **9**, 16 (2023).

[18] J. Nokkala, R. Martínez-Peña, G. L. Giorgi, V. Parigi, M. C. Soriano, and R. Zambrini, Commun. Phys. **4**, 53 (2021).

[19] K. Nakajima, K. Fujii, M. Negoro, K. Mitarai, and M. Kitagawa, Phys. Rev. Appl. **11**, 034021 (2019).

[20] J. Chen, H. I. Nurdin, and N. Yamamoto, Phys. Rev. Appl. **14**, 024065 (2020).

[21] R. Martínez-Peña, J. Nokkala, G. L. Giorgi, and J. Amato-Grill, Cogn. Comput. **15**, 1440 (2023).

[22] J. I. Latorre and M. A. Martín-Delgado, Phys. Rev. A **66**, 022305 (2002).

[23] R. O. Vallejos, F. de Melo, and G. G. Carlo, Phys. Rev. A **104**, 012602 (2021).

[24] D. E. Parker, X. Cao, A. Avdoshkin, T. Scaffidi, and E. Altman, Phys. Rev. X **9**, 041017 (2019).

[25] E. Rabinovici, A. Sánchez-Garrido, R. Shir, and J. Sonner, J. High Energy Phys. 06 (2021) 062.

[26] V. Balasubramanian, P. Caputa, J. M. Magan, and Q. Wu, Phys. Rev. D **106**, 046007 (2022).

[27] F. B. Trigueros and C.-J. Lin, SciPost Phys. **13**, 037 (2022).

[28] K. Adhikari, S. Choudhury, and A. Roy, Nucl. Phys. B **993**, 116263 (2023).

[29] Y. Shen, K. Klymko, J. Sud, D. B. Williams-Young, W. A. de Jong, and N. M. Tubman, Quantum **7**, 1066 (2023).

[30] M. Hochbruck and C. Lubich, SIAM J. Numer. Anal. **34**, 1911 (1997).

[31] B. N. Parlett, *The Symmetric Eigenvalue Problem: 20, Classics in Applied Mathematics* (Society for Industrial and Applied Mathematics, Philadelphia, PA, 1987).

[32] J. M. Ruffinelli, E. M. Fortes, D. A. Wisniacki, and M. Larocca, Phys. Rev. A **106**, 042423 (2022).

[33] B. Craps, O. Evnin, and G. Pascuzzi, Phys. Rev. Lett. **132**, 160402 (2024).

[34] A. Dymarsky and A. Gorsky, Phys. Rev. B **102**, 085137 (2020).

[35] X. Cao, J. Phys. A: Math. Theor. **54**, 144001 (2021).

[36] B. Bhattacharjee, P. Nandy, and T. Pathak, J. High Energy Phys. 08 (2023) 099.

[37] A. Bhattacharya, P. Nandy, P. P. Nath, and H. Sahu, J. High Energy Phys. 12 (2022) 081.

[38] B. Bhattacharjee, X. Cao, P. Nandy, and T. Pathak, J. High Energy Phys. 05 (2022) 174.

[39] B. L. Español and D. A. Wisniacki, Phys. Rev. E **107**, 024217 (2023).

[40] J. Barbón, E. Rabinovici, R. Shir, and R. Sinha, J. High Energy Phys. 10 (2019) 264.

[41] E. Rabinovici, A. Sánchez-Garrido, R. Shir, and J. Sonner, J. High Energy Phys. 03 (2022) 211.

[42] E. Rabinovici, A. Sánchez-Garrido, R. Shir, and J. Sonner, J. High Energy Phys. 07 (2022) 151.

[43] H. A. Camargo, V. Jahnke, H.-S. Jeong, K.-Y. Kim, and M. Nishida, Phys. Rev. D **109**, 046017 (2024).

[44] K. Hashimoto, K. Murata, N. Tanahashi, and R. Watanabe, J. High Energy Phys. 11 (2023) 040.

[45] G. Scialchi, A. Roncaglia, and D. A. Wisniacki (unpublished).

[46] I. García-Mata, R. A. Jalabert, and D. A. Wisniacki, Scholarpedia **18**, 55237 (2023).

[47] D. Gottesman, *Group22: Proceedings of the XXII International Colloquium on Group Theoretical Methods in Physics*, edited by S. P. Corney, R. Delbourgo, and P. D. Jarvis (International Press, Cambridge, 1999), pp. 32–43.

[48] R. Jozsa and M. V. den Nest, Quantum Inf. Comput. **14**, 633 (2013).

[49] R. Jozsa and A. Miyake, Proc. R. Soc. A **464**, 3089 (2008).

[50] D. J. Brod and A. M. Childs, Quantum Inf. Comput. **14**, 901 (2013).

[51] M. J. Bremner, R. Jozsa, and D. J. Shepherd, Proc. R. Soc. A **467**, 459 (2011).

[52] S. McArdle, S. Endo, A. Aspuru-Guzik, S. C. Benjamin, and X. Yuan, Rev. Mod. Phys. **92**, 015003 (2020).

[53] P. Jordan and E. Wigner, Eur. Phys. J. A **47**, 631 (1928).

[54] T. J. Park and J. Light, J. Chem. Phys. **85**, 5870 (1986).

[55] Y. Saad, SIAM J. Numer. Anal. **29**, 209 (1992).

[56] D. E. Stewart and T. Leyk, J. Comp. App. Math. **72**, 359 (1996).

[57] R. B. Sidje, ACM Trans. Math. Software **24**, 130 (1998).

[58] C. Moler and C. Van Loan, SIAM Rev. **45**, 3 (2003).

[59] T. Jawecki, W. Auzinger, and O. Koch, BIT Numer. Math. **60**, 157 (2020).

[60] F. Toscano and D. A. Wisniacki, Phys. Rev. E **74**, 056208 (2006).

[61] V. Oganesyan and D. A. Huse, Phys. Rev. B **75**, 155111 (2007).

[62] K. Kudo and T. Deguchi, Phys. Rev. B **97**, 220201(R) (2018).

[63] Y. Y. Atas, E. Bogomolny, O. Giraud, and G. Roux, Phys. Rev. Lett. **110**, 084101 (2013).

[64] O. Bohigas, M. J. Giannoni, and C. Schmit, Phys. Rev. Lett. **52**, 1 (1984).

[65] A. Bhattacharyya, D. Ghosh, and P. Nandi, J. High Energy Phys. 12 (2023) 112.

[66] C. Liu, H. Tang, and H. Zhai, Phys. Rev. Res. **5**, 033085 (2023).

[67] https://github.com/laiadc/Krylov_QR/